Wavelength measurements of heliumlike $1s2s\ ^3S_1-1s2p\ ^3P_{0,2}$ transitions in Ne^{8+}, Na^{9+}, Mg^{10+}, and Si^{12+} emitted by solar flare plasmas

W. Curdt, E. Landi, and K. Wilhelm
Max-Planck-Institut für Aeronomie, D-37191 Katlenburg-Lindau, Germany

U. Feldman
E. O. Hulburt Center for Space Research, Naval Research Laboratory, Washington, D.C. 20375

(Received 25 January 2000; published 5 July 2000)

With the Solar Ultraviolet Measurements of Emitted Radiation instrument—a high-resolution normal-incidence telescope and spectrometer on board the Solar and Heliospheric Observatory—heliumlike $1s2s\ ^3S_1-1s2p\ ^3P_{0,2}$ transitions in the highly ionized species Ne^{8+}, Na^{9+}, Mg^{10+}, and Si^{12+} were observed. The spectral lines were emitted by high-temperature solar flare plasmas. In this paper, we report on wavelength measurements of the He-like lines identified in the recorded spectra. The wavelength uncertainties we obtained from the solar measurements are $\leqslant 20$ mÅ(1σ), and in one case $\leqslant 30$ mÅ. This is comparable to or better than the best determinations so far achieved for these heliumlike $1s2s\ ^3S_1-1s2p\ ^3P_{0,2}$ transitions with instrumentation in the laboratory. For the $Na^{9+}\ ^3S_1-^3P_2$ transition we report what is to our knowledge the first wavelength measurement. The knowledge of the accurate wavelengths can provide important checks on atomic structure calculations.

PACS number(s): 32.30.Jc, 95.30.Ky, 95.55.Qf, 96.60.Tf

I. INTRODUCTION

High-accuracy wavelength measurements of heliumlike $1s2s\ ^3S_1-1s2p\ ^3P_{0,2}$ transitions are being used as benchmarks for *ab initio* tests of relativistic and radiative atomic structure calculations. In the past decade, the energies of low-lying levels in He-like ions were the focus of extensive theoretical calculations. Recently Berry, Dunford, and Livingston [1] and Kukla *et al.* [2] published comparisons between experimental measurements and theoretical calculations of the $1s2s\ ^3S_1-1s2p\ ^3P_{0,2}$ transition energies in many elements with atomic numbers, Z, between 3 and 92. They have shown that in the case of the $1s2s\ ^3S_1-1s2p\ ^3P_2$ transitions—to within the experimental uncertainties—good agreement exists between the experimental values and the theoretical calculations of Drake [3] in 1988, but a discrepancy of the order of 2.3 $(Z/10)^4$ cm^{-1} prevails in the $1s2s\ ^3S_1-1s2p\ ^3P_0$ transitions. The authors in Refs. [1] and [2] have also demonstrated that the discrepancies between experimental results and more accurate relativistic calculations of a new generation [4–6] practically disappear.

In this paper, we discuss wavelength measurements of the $1s2s\ ^3S_1-1s2p\ ^3P_{0,2}$ transitions in the ions Ne^{8+}, Na^{9+}, Mg^{10+}, and Si^{12+}. The Ne^{8+} transition energies and wavelengths were measured before in a number of laboratory experiments. The results with the smallest uncertainty of 20 mÅ were reported by Brown *et al.* [7] and Beyer, Folkmann, and Schartner [8]. No measurements of the Na^{9+} transition energies are available to our knowledge. Wavelengths of Mg^{10+} were measured in a beam foil experiment by Klein *et al.* [9]. The authors claim an uncertainty of ≈ 80 mÅ. Transitions of Si^{12+} were also measured before in laboratory experiments by DeSerio *et al.* [10] and Howie *et al.* [11]. In both sets of measurements the $1s2s\ ^3S_1-1s2p\ ^3P_0$ transition wavelengths were determined to an uncertainty of 30 mÅ and the $1s2s\ ^3S_1-1s2p\ ^3P_2$ transition wavelengths to an uncertainty of 20 mÅ. Although not explicitly stated in all the references, it is assumed that uncertainties have been quoted as 1σ values.

In the present work, we present solar observations obtained from a space instrument that allowed us to determine a new set of wavelength measurements of most of the $1s2s\ ^3S_1-1s2p\ ^3P_{0,2}$ transitions in Ne^{8+}, Na^{9+}, Mg^{10+}, and Si^{12+}. The wavelength uncertainties of the new measurements are comparable to and in some cases better than those attained in the laboratory. When converting the uncertainties of our measurements from wavelengths to energy units, the derived values vary between 0.4 $(Z/10)^4$ and 1.4 $(Z/10)^4$ cm^{-1}.

In Sec. II we describe the space-based instrument that was used to record the spectra. Section III deals with the types of solar plasmas which are expected to emit sufficiently bright $1s2s-1s2p$-type transitions from medium Z elements. Section IV describes the observations analyzed in the present work. The detailed measurements are described in Sec. V, and in Sec. VI we present the conclusions.

II. THE INSTRUMENT

The Solar Ultraviolet Measurements of Emitted Radiation (SUMER) instrument is a high-resolution telescope and spectrometer on board the Solar and Heliosperic Observatory (SOHO). The SOHO spacecraft orbits around the first Lagrange point, L_1, in continuous view of the Sun and is an ideal platform for solar observations. The instrument has been described in detail by Wilhelm *et al.* [12]. Below we present only the instrumental details that are pertinent to understanding the measurements discussed in this paper.

SUMER records high-resolution spectra emitted by solar plasmas. The telescope mirror can be moved in two perpendicular directions and can image any point within a 64 arcmin×64 arcmin field of view on the entrance slit.

The spectrometer consists of the entrance slit, an off-axis parabola mirror, which collimates the light leaving the slit, a flat mirror, which deflects the light onto a grating, and a 3600-line mm^{-1}, 3200-mm radius spherical grating. The grating, which is arranged in a Wadsworth configuration, directs the light into one of two imaging detectors. The two detectors can be used alternatively to collect stigmatic images of the slit. Detector A covers the wavelength range from 780 Å to 1610 Å in first order, detector B from 660 Å to 1500 Å, respectively. Second-order lines are superimposed on the first-order spectrum. Each detector has an array of 1024 (spectral) ×360 (spatial) pixels which covers a spectral range of ≈43 Å in first order. The angular scale of a pixel is ≈1 arcsec. In the first-order spectrum, a pixel corresponds to ≈43 mÅ.

The SUMER optics are made of silicon carbide, which is a fairly good reflector for radiation with wavelengths longer than 500 Å. In principle, the second-order spectrum, which is superimposed on the first-order spectrum, should cover the 390-Å to 805-Å range for detector A. However, due to the fact that SUMER uses four reflections, three at normal incidence and one at grazing incidence, the responsivity of the instrument for wavelengths below 500 Å is very low.

With SOHO in its nominal attitude, the SUMER instrument is oriented with its slit aligned along the north-south direction. During most of the observations presented here, the 1×300 $arcsec^2$ slit was used and all spectra have been exposed for 300 s. In two cases the 4×300 $arcsec^2$ slit was in operation.

The detector photocathode consists of a microchannel plate with sections of different surface coatings. On both sides of the microchannel plate, ≈250 pixels are uncoated while the center pixels (≈500) are coated with KBr. The efficiency of the detector section coated with KBr is higher than the efficiency of the uncoated parts over most of the wavelength range. Therefore, a comparison of the intensity of a particular line recorded on the KBr with its intensity obtained from the uncoated part of the detector can reveal unambiguously if a line is seen in first or second order.

When spectral information is gathered off the disk from plasmas located high above the solar limb, in addition to genuine lines emitted by the line-of-sight coronal plasmas, lines that are scattered into the spectrometer slit by imperfections on the front mirror are also present. The scattered lines are produced by bright resonance transitions of neutrals and singly or doubly ionized species that are very abundant in cold solar plasmas. Since the wavelengths of many such lines are very accurately known (cf., e.g., the line lists of Feldman *et al.* [13] and Curdt *et al.* [14], and references therein), and since they are not affected by measurable net bulk motions of the emitting plasma, they provide ideal wavelength references.

III. THE PLASMA CONDITIONS IN THE SOLAR ATMOSPHERE

The solar atmosphere consists of plasmas having vastly different properties. The coldest solar plasmas from which molecular lines are often detected have a temperature of $\approx 3\times10^3$ K (cf., Schühle *et al.* [15]). When the solar activity cycle is near its minimum, the temperature of coronal plasmas seldom exceeds 1.5×10^6 K. However, when the solar cycle is at its most active phase and during solar flares, the temperature can reach 3×10^7 K. At such temperatures the only elements which are not, to a large extent, fully ionized are those having atomic numbers of $Z\geqslant 18$. Due to this situation, during solar minimum, lines emitted by ions that are typically present in plasmas having temperatures in the $3\times10^4\ \mathrm{K}<T_e<1.5\times10^6$ K range are detected; during solar maximum, lines associated with any ion that is expected to exist in plasmas with temperatures in the $3\times10^4\ \mathrm{K}<T_e<3\times10^7$ K range can be observed.

Wavelength calculations indicate that SUMER in its wavelength range should be able to record transitions from He-like ions between F ($Z=9$) and Ti ($Z=22$). In reality this is not the case, because the detected intensity of the $1s2s-1s2p$ He-like transitions in solar spectra depend on several other factors. In addition to its dependence on the instrumental efficiency, the probability of detecting a particular transition is a function of the plasma conditions; most importantly it depends on the elemental abundance in the solar atmosphere, on the plasma temperature, T_e, on the electron density, N_e, and on the amount of plasma along the line of sight, $\int N_e dh$. The solar physics literature commonly refers to the quantity described by the integral $\int N_e^2 dh$ as the *emission measure*. The solar coronal abundances relative to Mg ($Z=12$) of elements in the $9\leqslant Z\leqslant 22$ range are given in Table I. For details on the elemental abundance in coronal plasmas, see Feldman [16] and Feldman and Laming [17]. The table also gives the temperatures at which the He-like ions of the most abundant elements reach their maximum fractional abundance under coronal equilibrium conditions. As shown in the table, the only He-like lines most likely expected to be present in coronal plasmas would belong to the Ne IX, Na X, Mg XI, Al XII, Si XIII, S XV, Ar XVII, and Ca XIX spectra.

Although the temperature conditions required to ionize Ne, Na, and Mg to the He-like stage are found even in nonflaring active regions, in reality the lines are seldom seen in such plasmas. One of the reasons for this is the unusually high excitation energy, ΔE, of the upper levels ($1s2p\ ^3P_{0,2}$) of the He-like transitions above the ground states. The collisional excitation cross section into the $1s2p\ ^3P_{0,2}$ levels, in optically thin low-density plasmas, is proportional to the factor $T_e^{-1/2}\exp(-\Delta E/kT_e)$, where k is the Boltzmann constant. When substituting the actual excitation energies and temperatures of maximum fractional abundance in the equation, the values of the quantity $\Delta E/(kT_M)$ become quite large (see Table I), resulting in very small excitation cross sections.

It is only when the electron temperature in the plasma is significantly higher than required to ionize the element to the He-like degree of ionization that the cross sections become sufficiently large to populate the $1s2p\ ^3P_{0,2}$ levels. Such conditions usually happen in flaring plasmas. Furthermore, the electron densities in these plasmas are typically a few

TABLE I. Abundances in solar coronal plasmas relative to Mg for elements in the $9 \leqslant Z \leqslant 22$ range. The electron temperatures of maximum fractional abundance, T_M, needed to produce the He-like ionization stage in coronal plasmas, are given in column 4 for the most abundant elements in the solar corona. In column 5 we present the exponent of the Boltzmann factor for their He-like transitions.

Element	Atomic Number Z	Elemental abundance [a]	T_M [b] (10^6 K)	$\frac{\Delta E}{kT_M}$
F	9	1×10^{-3}		
Ne	10	8×10^{-1}	1.3	8.2
Na	11	6×10^{-2}	2.0	6.5
Mg	12	1.0	2.5	6.3
Al	13	8×10^{-2}	3.1	6.0
Si	14	9×10^{-1}	4.0	5.4
P	15	2×10^{-3}		
S	16	1×10^{-1}	6.3	4.5
Cl	17	1×10^{-3}		
Ar	18	2×10^{-2}	9.0	4.0
K	19	3×10^{-3}		
Ca	20	6×10^{-2}	13.0	3.5
Sc	21	4×10^{-5}		
Ti	22	3×10^{-3}		

[a]The reported relative elemental abundances are for typical coronal plasmas, which are different from normal photospheric abundances. For details on elemental abundances in solar coronal plasmas, see Feldman [16] and Feldman and Laming [17].

[b]Temperatures and relative excitation energies are given only for elements with coronal abundances that are at least 1% of the Mg abundance.

orders of magnitude higher than in the nonflaring corona resulting in relatively large emission measures. Therefore, the best opportunity for detecting the Ne IX, Na X, Mg XI, Al XII, and Si XIII $1s2s\ ^3S_1-1s2p\ ^3P_{0,2}$ lines is in spectra emitted by moderate-sized flares. The best chance to detect S XV, Ar XVII, and Ca XIX lines is in spectra emitted by very energetic flares.

So far, SUMER acquired spectra from only a few moderate-sized flares. Therefore, the only well-exposed lines of this category, which we detected up to now, belong to Ne IX, Na X, Mg XI, and Si XIII. The ionic fractions and the normalized contribution functions of these species are displayed in Fig. 1, illustrating the effect of the high excitation energies of the upper levels.

IV. THE OBSERVATIONS

Several data sets have been evaluated in order to measure accurate wavelengths of the He-like transitions. Standard procedures have been applied for the basic data processing, i.e., decompression, flat-field correction, and geometrical distortion correction. Special attention has been paid to the spectra covering the whole SUMER spectral range recorded on May 9, 1999 and November 5, 1999. Their importance is given by the fact that $^3S_1-^3P_{0,2}$ transitions from He-like ions from Ne, Na, Mg, and Si have been observed as strong

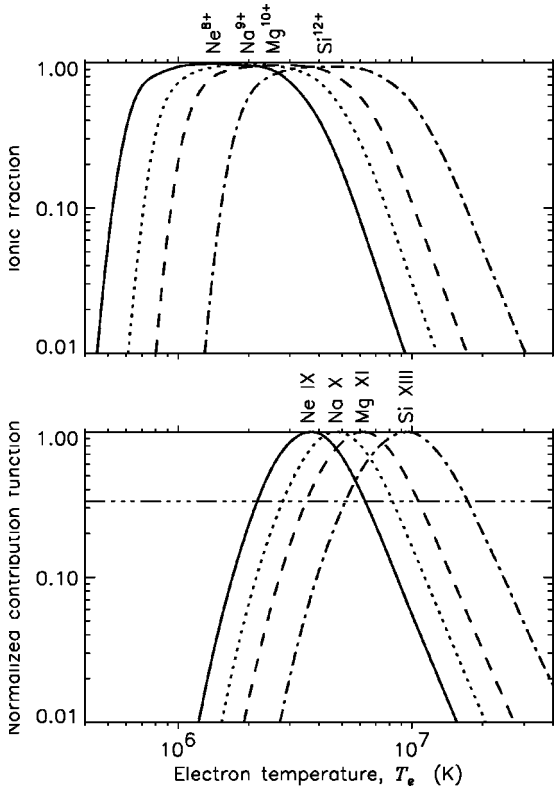

FIG. 1. Comparison of the ionic fractions of Ne^{8+}, Na^{9+}, Mg^{10+}, and Si^{12+} interpolated from Arnaud and Rothenflug [18] (top) and the normalized contribution functions of the corresponding spectral lines (bottom). The cutoff at low temperatures caused by the high excitation energy of the upper levels can clearly be seen. At one-third of the maximum, a horizontal line is drawn indicating at which temperatures substantial contributions to the lines can be expected.

lines. In all the other data sets considered, only a few of these lines have been detected.

A. The May 9, 1999 flare observations

On May 9, 1999 at about 17:53 UT, a solar flare of size M 7.6 erupted above the active region NOAA 8537, which was approaching the solar west limb. The x-ray flux from the flare, as monitored by the GOES 8 satellite,[1] peaked at about 18:07 UT and since then it began its decay. By 19:00 UT, the x-ray flux had dropped by over an order of magnitude from its maximum and by 21:00 UT it dropped by another factor of 2 to 3 until it could no longer be distinguished from the solar x-ray background. When the flare erupted, SUMER was in a so-called Reference Spectrum mode, in which the instrument scanned with some overlap the entire wavelengths range in $\approx$43 Å sections, recording with detector A. At flare onset the detector recorded spectra near 1395 Å while advancing towards longer wavelengths. At the time of peak x-ray flux, the detector recorded the spectrum around

[1]Available at http://sel.noaa.gov/today.html

1450 Å and by about 18:44 UT it reached the upper limit of the spectral range ($\approx$1600 Å), at which point the spectrometer restarted its operation from the 800 Å position. It completed the second full spectral scan at about 22:00 UT. A less intense flare of size C 5.1 occurred at 16:09 UT, when the instrument recorded the spectrum around 980 Å.

Although it is not clear that the spectrometer slit was imaging the hottest portion of the flare, it definitely detected radiation emitted by hot flaring plasmas, as witnessed by the Fe XX, Fe XXI, and Fe XXIII lines that are present in the recorded spectra and evidence of $\geqslant 10^7$ K temperatures. The active region which the SUMER slit was pointing at during the May 9, 1999 observations was a site of continuous flare activity. Therefore, even prior to the onset of the main flare, lines belonging to the Ne IX, Na X, Mg XI, and Si XIII spectra were detected, although they were not as intense as later during the main phase of the flare. In the following, we will refer to the first of these two Reference Spectra as FLARE1 and to the second as FLARE2.

B. The May 1999 flare dynamics campaign

During the first week in May 1999, when SUMER was participating in a coordinated flare dynamics campaign, several other observations were performed. On May 3, 1999, SUMER recorded multiple full spectral scans above active region NOAA 8524, which was approaching the west limb. Ne IX emission was observed from this nonflaring site. On May 4 and May 5, this target was selected for long time series in selected spectral bands. In one of the bands the 1043 Å Mg XI line was present.

On May 9, 1999, more time series were obtained before and after the May 9 flare mentioned above. From 12:08 UT to 15:22 UT and from 22:10 UT to 07:55 UT no flares were reported for active region NOAA 8537, although the emitting plasma must have been still at high temperatures. Emission from Na X and Mg XI was observed in the spectral bands from 1098 Å to 1138 Å and from 1040 Å to 1060 Å. All spectra were recorded with detector A.

C. The October/November 1999 flare campaign

On November 5, 1999, using detector A, a full spectral scan was performed from 21:14 UT to 00:28 UT in the postflare loops above active NOAA 8759, which at that time was located at the east limb. While bright Doppler-shifted emission from relatively cold ions (transition region plasma, 3×10^4 K$<T_e<1\times10^6$ K) is observed in the loops, other sections along the slit are dominated by very hot plasma ($T_e>10^7$ K). The lines of interest are all present in this data set, which we will refer to as FLARE3.

D. Other spectra

The paper on high-temperature lines by Feldman *et al.* [19] deals with lines of Ar XII, Ar XIII, Ca XIII, Ca XIV, Ca XV, Fe XVII, Fe XVIII, Fe XIX, Ni XIII, Ni XIV, and Ni XV, based on a data set recorded with detector B on September 6, 1997. At that time a full spectral scan was obtained above active region NOAA 8076. We reanalyzed the spectra and found also emission from He-like ions not reported in Ref. [19].

The analysis of the first ionization potential (FIP) effect by Dwivedi, Curdt, and Wilhelm [20] was based on an off-limb raster in the spectral band from 980 Å to 1020 Å above the nonflaring active region NOAA 7974 on June 20, 1996, starting at 20:11 UT. As we have found now, emission of the 997.5 Å Mg XI line is present in this detector A data set.

V. EXPERIMENTAL RESULTS

A comprehensive review of results from previous determinations of He-like transition energies was published by Kukla *et al.* [2]. We have included in Table II the pertinent information regarding the $1s2s\ ^3S_1-1s2p\ ^3P_0$ and the $1s2s\ ^3S_1-1s2p\ ^3P_2$ transitions of Ne IX, Na X, Mg XI, and Si XIII. In the cases of Ne IX and Si XIII, we have quoted experimental values only from the most accurate measurements. Table II also includes the three most recent theoretical results of the two transitions for the ions of interest.

We have measured He-like wavelengths from FLARE1, FLARE2, and FLARE3 data sets, as they were the only ones where lines of all the ions listed in Table II were detected in flare observations. Due to the overlapping spectral windows, each line is normally found in two spectra. In a few cases (Ne IX $^3S_1-^3P_2$, Na X $^3S_1-^3P_2$, and Mg XI $^3S_1-^3P_0$), multiple observations are available, providing 11, 27, and 7 wavelength measurements, respectively. Thus, we have reported in Table II the averages of these measurements as final wavelengths, with their standard deviations as uncertainties.

The wavelength-to-pixel relation in SUMER spectra changes in different observations, and so it needs to be calibrated for each exposure. This is achieved by using transitions of lines simultaneously observed as reference in the selected spectral range. These calibration lines must satisfy the following requirements: no systematic Doppler shifts should be present along the line of sight, and their wavelengths need to be known with high accuracy.

In all our data sets, the field of view of the instrument was placed outside the solar disk. In this case, taking into account the properties of the solar atmosphere and the SUMER spectrometer, lines from neutral or singly ionized species, seen as scattered light from the disk, provide the best reference lines. In those cases, where not enough cold lines were available in the selected spectral range, the second best choice is provided by hot coronal lines, emitted by plasma outside magnetic loop structures. In order to obtain the wavelength-to-pixel relation of a given SUMER frame, the relation between the fitted line centroids of the reference lines and wavelength is approximated with a quadratic curve to account for instrumental nonlinearities by a least-square fit. Note that the dispersion in the focal plane is a nonlinear function along the spectral axis [12].

For each of the three lines (Ne IX $^3S_1-^3P_2$, Na X $^3S_1-^3P_2$, and Mg XI $^3S_1-^3P_0$), where many observations were available, the presence of a strong reference line lying very close to the He-like line ($|\Delta\lambda|\leqslant 2$ Å) allows us to measure the He-like wavelength in a simpler way, namely by

TABLE II. Calculated and measured wavelengths belonging to the He-like transitions $1s2s\ ^3S_1-1s2p\ ^3P_0$ and $1s2s\ ^3S_1-1s2p\ ^3P_2$. Wavelengths are in Å, and uncertainties are given as 1σ values (see text).

	Ne^{8+}		Na^{9+}		Mg^{10+}		Si^{12+}	
	$^3S_1-^3P_0$	$^3S_1-^3P_2$	$^3S_1-^3P_0$	$^3S_1-^3P_2$	$^3S_1-^3P_0$	$^3S_1-^3P_2$	$^3S_1-^3P_0$	$^3S_1-^3P_2$
				Calculated wavelengths				
J[a]	1277.738	1248.098			1043.319	997.486	878.665	814.710
C[b]	1277.702	1248.065			1043.298	997.455	878.646	814.693
P[c]	1277.705	1248.065	1149.202	1111.765	1043.303	997.460	878.652	814.698
				Laboratory wavelengths				
Expt.	1277.68±0.04[d]	1248.12±0.02[d]			1043.29±0.08[e]	997.38±0.08[e]	878.63±0.03[f]	814.69±0.02[f]
Expt.	1277.71±0.02[g]	1248.15±0.02[g]					878.68±0.03[h]	814.71±0.02[h]
Expt.		1248.07±0.02[i]						
				Newly measured wavelengths from solar flare spectra				
Fl. 1						997.456±0.030	878.667±0.052	814.746±0.048
Fl. 2						997.430±0.030	878.683±0.062	814.728±0.044
Fl. 3						997.461±0.042	878.696±0.040	814.716±0.035
Avg.		1248.101±0.013		1111.770±0.017	1043.283 ±0.010	997.448±0.019	878.683±0.029	814.728±0.024

[a]Wavelengths based on calculations by Johnson and Sapirstein [4].
[b]Wavelengths based on calculations by Chen, Cheng, and Johnson [5].
[c]Wavelengths based on calculations by Plante, Johnson, and Sapirstein [6].
[d]Wavelengths from measurements by Engelhardt and Sommer [21].
[e]Wavelengths from measurements by Klein *et al.* [9].
[f]Wavelengths from measurements by DeSerio *et al.* [10].
[g]Wavelengths from measurements by Brown *et al.* [7].
[h]Wavelengths from measurements by Howie *et al.* [11].
[i]Wavelengths from measurements by Beyer, Folkmann, and Schartner [8].

assuming a constant dispersion in the given small spectral range and using the pixel centroids of the two lines. The constant dispersion is known from the optical design of the instrument. This method—here referred to as the direct dispersion method—has the advantage of eliminating any uncertainties of the quadratic fit. Thanks to the availability of many observations for each line, the final wavelength values are obtained averaging the wavelengths from single observations. It is thus possible to eliminate any potential systematic bias due to bulk plasma motions.

Since we are observing off the limb, we have to take the Doppler effect of the solar rotation into account. Assuming zero Doppler flow in lines observed as scattered light from the disk and a rigid body rotation of 2 km s^{-1} at the equator, we arrive at Doppler shifts of ±5 mÅ at 814 Å and ±8 mÅ at 1248 Å. We have corrected our results for this offset.

A. Ne IX transitions

The Ne IX $^3S_1-^3P_0$ line is listed by Kelleher *et al.* [22] with a wavelength of 1277.79 Å. But in solar plasmas the second-order Si X line at 638.94 Å is blending the weak Ne IX line. This makes it difficult to accurately fit the Ne IX line and therefore it was not measured.

The Ne IX $^3S_1-^3P_2$ transition has been observed in 11 different spectra. The presence of the very strong Mg X $2s\ ^2S_{1/2}-2p\ ^2P_{1/2}$ second-order line allows us to use the direct dispersion method. The literature value of 624.943 Å for this line from Behring *et al.* [23] led to significant deviations from both the laboratory measurements and the theoretical calculations. Recent work of Peter and Judge [24] and Dammasch *et al.* [25], also based on SUMER data, indicates that the wavelength determination in Ref. [23] was somewhat too short. They found wavelengths of (624.968±0.007) Å and (624.965±0.003) Å, respectively, in independent studies. This excellent agreement within the small uncertainty margins demonstrates that SUMER observations can be used for accurate rest wavelength determinations. In addition, comparable uncertainties were obtained for Ne VIII at 770 Å [26].

The Si X $2s^22p\ ^2P_{3/2}-2s2p^2\ ^4P_{5/2}$ line, which is listed in Ref. [22] at 624.729 Å, is observed as a resolvable blend in the blue wing of the Mg X line and can be used as an additional check. We found Si X shorter than Mg X by (254 ±8) mÅ. With 624.965 Å for Mg X, we get (624.711 ±0.11) Å for Si X, which seems to be compatible with the quoted value.

We also used the quadratic fit procedure to measure the Ne IX and Si X transition wavelengths. Several reference lines were available, and the results we obtained are in close agreement with the literature wavelengths for both ions. The resulting wavelength of both methods listed in Table II is (1248.101±0.013) Å, which is in reasonable agreement with the literature values. The uncertainty, given by the standard deviation, is lower than in the previous studies.

B. Na X transitions

No trace is found of the Na X $^3S_1-^3P_0$ line in the present data set. The Na X $^3S_1-^3P_2$ line is isolated and close to the Si III $3s3p\ ^3P_2-3s3d\ ^3D_2$ line at 1113.230 Å, whose presence is caused by the chromospheric light scattered in the

instrument. The presence of Si III has allowed us to apply again the direct dispersion method. The reference value for the Si III wavelength is taken from Ref. [22]. The Na X $^3S_1-^3P_2$ transition has been observed in 27 spectra and this has permitted the calculation of its wavelength as the average of the measured wavelengths. The resulting value is in good agreement with theoretical estimates. To our knowledge, this is the first wavelength measurement of this line.

C. Mg XI transitions

Both the Mg XI $^3S_1-^3P_2$ and $^3S_1-^3P_0$ lines have been observed in our data sets. The $^3S_1-^3P_0$ line is isolated and lies very close to the strong second-order Si XII $2s\,^2S_{1/2}-2p\,^2P_{1/2}$ transition at 520.665 Å, which is taken as reference and allows the use of the direct dispersion method. The Si XII wavelength value is again taken from Kelleher *et al.* [22].

The Mg XI $^3S_1-^3P_0$ line has been detected in seven spectra, over which the measured wavelengths have been averaged. This line was present in four other spectra, but its weakness caused the line profile fit to be uncertain, so these measurements were discarded. The averaged $^3S_1-^3P_0$ wavelength value is in reasonable agreement with previous theoretical and laboratory estimates. The uncertainty (given by the standard deviation) is considerably lower than in previous studies. Other SUMER studies [24–26] have shown that systematic offsets—e.g., residual detector nonlinearities or thermoelastic effects of the spectroscope—are not a concern, unless uncertainties of less than 3 mÅ are required.

The Mg XI $^3S_1-^3P_2$ line is strong and apparently isolated, and in principle should be detectable in several nonflaring data sets. Indeed, this line has been detected by Dwivedi, Curdt, and Wilhelm [20] in off-disk spectra recorded above active regions, although they report it as unidentified. However, the wavelength they measured is considerably far ($\approx$140 mÅ) from the previous theoretical and laboratory measurements reported in Table II, thus suggesting that this line might be blended with an unidentified line. We have found the Mg XI $^3S_1-^3P_2$ line in several other data sets, but in nearly all of them the wavelength was close to the value in Ref. [20]. Only in flaring plasmas did we measure wavelengths in good agreement with the previous estimates, and this suggests that in nonflaring plasma the Mg XI transition is blended with a cooler line, the contribution of which becomes negligible in hotter plasma. We have investigated possible identifications of this line and suggest that a Fe III line at 997.599 Å is present (cf., Ref. [14]) in the data set of Dwivedi, Curdt, and Wilhelm [20] as an unresolvable blend leading to the observed redshift of the Mg XI line, since several other lines of Fe III were found in their data set.

Therefore, the only reliable measurements for the $^3S_1-^3P_2$ wavelength are those from the FLARE1, FLARE2, and FLARE3 data sets, reported in Table II. The uncertainties of the individual measurements have contributions from fitting the line centroid and from the wavelength calibration. In the last row we listed the weighted average of the individual measurements and the resulting uncertainty, derived by error propagation considerations (also for Si XIII transitions). Our uncertainty is much lower compared to the results in Ref. [9].

D. Si XIII transitions

Both of the Si XIII transitions are detected in the FLARE1, FLARE2, and FLARE3 data sets, but they are not seen in spectra emitted by nonflaring plasma.

The Si XIII $^3S_1-^3P_0$ line is weak and only very few reference lines are available in the spectral range of the $^3S_1-^3P_0$ line, so that each individual wavelength calibration is not very accurate. In addition, this line is blended with a S IX line, listed in Ref. [13] at 878.81 Å, and an unidentified blend in the blue wing. Both blends can be resolved by a multi-Gauss fit, but this introduces another systematic error for which a conservative value of 20 mÅ has been assumed. From the results in Table II, it is seen that all individual measurements are in general agreement with previous theoretical and laboratory measurements thanks to the relatively large uncertainties. The uncertainty of the weighted average, however, is not larger than the value quoted in Ref. [10] or Ref. [11].

The Si XIII $^3S_1-^3P_2$ line can be measured more easily as the line is stronger and well detected. This line is, again, blended in the blue wing and treated with a multi-Gauss fit. The blend is identified in Ref. [13] as Ar IX with a question mark and listed at 814.52 Å. The wavelength values, reported in Table II, are in agreement with the literature values, and the uncertainties are comparable to those obtained in laboratory measurements.

VI. CONCLUSIONS

In the present work, we have measured six out of eight wavelengths of the $1s2s\,^3S_1-1s2p\,^3P_{0,2}$ transitions of the He-like ions Ne IX, Na X, Mg XI, and Si XIII from high-resolution spectra of solar flares using the SUMER instrument on board of SOHO. To our knowledge, the Na X $^3S_1-^3P_2$ wavelength was measured for the first time. We have compared our wavelength measurements with previous laboratory values and with theoretical calculations from atomic models and found good agreement. The uncertainties in our measurements are comparable to or smaller than those achieved in laboratory spectra; when converted into energy units, our uncertainties lie between $0.4\,(Z/10)^4$ and $1.4\,(Z/10)^4$ cm^{-1}.

It seems that solar plasmas are a very useful source of far-ultraviolet emission lines, which can be used for accurate wavelength measurements. Assuming that net flows of the emitting plasmas can be excluded, the limitation comes from line blending problems and the availability and reliability of good reference wavelengths. Our study supports the findings requiring a revision of the rest wavelength of the Li-like Mg X $2s\,^2S_{1/2}-2p\,^2P_{1/2}$ transition at 624.9 Å.

ACKNOWLEDGMENTS

The SUMER project is financially supported by DLR, CNES, NASA, and the ESA PRODEX Program (Swiss contribution). SUMER is part of SOHO, the Solar and Heliospheric Observatory, of ESA and NASA. The work of Uri Feldman was supported by the ONR/NRL Research Option, Solar Magnetism and Earth's Environment and by a NASA SR&T grant.

[1] H.G. Berry, R.W. Dunford, and A.E. Livingston, Phys. Rev. A **47**, 698 (1993).
[2] K.W. Kukla, A.E. Livingston, J. Suleiman, H.G. Berry, R.W. Dunford, D.S. Gemmell, E.P. Kanter, S. Cheng, and L.J. Curtis, Phys. Rev. A **51**, 1905 (1995).
[3] G.W.F. Drake, Can. J. Phys. **66**, 586 (1988).
[4] W.R. Johnson and J. Sapirstein, Phys. Rev. A **46**, R2197 (1992).
[5] M.H. Chen, K.T. Cheng, and W.R. Johnson, Phys. Rev. A **47**, 3692 (1993).
[6] D.R. Plante, W.R. Johnson, and J. Sapirstein, Phys. Rev. A **49**, 3519 (1994).
[7] J.S. Brown, C.W. Band, E.C. Finch, R.A. Holt, H.A. Klein, J. Laursen, A.F. McClelland, N.J. Peacock, J.D. Silver, M.F. Stamp, and J. Takacs, Nucl. Instrum. Methods Phys. Res. B **9**, 682 (1985).
[8] H.F. Beyer, F. Folkmann, and K.-H. Schartner, Z. Phys. D: At., Mol. Clusters **1**, 65 (1986).
[9] H.A. Klein, F. Moscatelli, E.G. Myers, E.H. Pinnington, J.D. Silver, and E. Träbert, J. Phys. B **18**, 1483 (1985).
[10] R. DeSerio, H.G. Berry, R.L. Books, J. Hardis, A.E. Livingston, and S.J. Hinterlong, Phys. Rev. A **24**, 1872 (1981).
[11] D.J.H. Howie, W.A. Hallett, E.G. Myers, D.D. Dietrich, and J.D. Silver, Phys. Rev. A **49**, 4390 (1994).
[12] K. Wilhelm *et al.*, Sol. Phys. **162**, 189 (1995).
[13] U. Feldman, W.E. Behring, W. Curdt, U. Schühle, K. Wilhelm, P. Lemaire, and T.M. Moran, Astrophys. J., Suppl. **113**, 195 (1997).
[14] W. Curdt, U. Feldman, J.M. Laming, K. Wilhelm, U. Schühle, and P. Lemaire, Astron. Astrophys., Suppl. Ser. **126**, 281 (1997).
[15] U. Schühle, C.M. Brown, W. Curdt, and U. Feldman, in *Proceedings of the 8th SOHO Workshop, Paris, 1999*, edited by J.-C. Vial and B. Kaldeich-Schürmann (ESA-SP, Paris, 1999), Vol. 446, p. 617.
[16] U. Feldman, Phys. Scr. **46**, 202 (1992).
[17] U. Feldman and J.M. Laming, Phys. Scr. **61**, 222 (2000).
[18] M. Arnaud and R. Rothenflug, Astron. Astrophys., Suppl. Ser. **60**, 425 (1985).
[19] U. Feldman, W. Curdt, G.A. Doschek, U. Schühle, K. Wilhelm, and P. Lemaire, Astrophys. J. **503**, 467 (1998).
[20] B.N. Dwivedi, W. Curdt, and K. Wilhelm, Astrophys. J. **517**, 516 (1999).
[21] W. Engelhardt and J. Sommer, Astrophys. J. **167**, 201 (1971).
[22] D.E. Kelleher, P.J. Mohr, W.C. Martin, W.L. Wiese, J. Sugar, J.R. Fuhr, K. Olsen, A. Musgrove, J. Reader, C.J. Sansonetti, and G.R. Dalton, Proc. SPIE **3818**, 170 (1999).
[23] W.E. Behring, L. Cohen, U. Feldman, and G.A. Doscheck, Astrophys. J. **203**, 521 (1976).
[24] H. Peter and P.G. Judge, Astrophys. J. **522**, 1148 (1999).
[25] I.E. Dammasch, D.M. Hassler, K. Wilhelm, and W. Curdt, in *Proceedings of the 8th SOHO Workshop, Paris, 1999* (Ref. [15]), p. 263
[26] I.E. Dammasch, K. Wilhelm, W. Curdt, and D.M. Hassler, Astron. Astrophys. **346**, 285 (1999).